
BAYESIAN MODELING OF DYNAMIC BEHAVIORAL CHANGE DURING AN EPIDEMIC

CAITLIN WARD^{1,*}, ROB DEARDON^{2,3}, ALEXANDRA M. SCHMIDT⁴

¹ Division of Biostatistics, University of Minnesota

² Faculty of Veterinary Medicine, University of Calgary

³ Department of Mathematics and Statistics, University of Calgary

⁴ Department of Epidemiology, Biostatistics, and Occupational Health, McGill University

ABSTRACT

For many infectious disease outbreaks, the at-risk population changes their behavior in response to the outbreak severity, causing the transmission dynamics to change in real-time. Various approaches to incorporating behavioral change in epidemic models have been proposed, but work assessing the statistical properties of these models in relation to real data is limited. We propose a model formulation where time-varying transmission is captured by the level of “alarm” in the population and specified as a function of the past epidemic trajectory. The model is set in a data-augmented Bayesian framework as epidemic data are often only partially observed, and we can utilize prior information to help with parameter identifiability. We investigate the estimability of the population alarm across a wide range of scenarios, using both parametric functions and non-parametric splines and Gaussian processes. The benefit and utility of the proposed approach is illustrated through an application to COVID-19 data from New York City.

Keywords Bayesian inference · COVID-19 · SIR · Transmission modeling

1 Introduction

Human behavior is a driving factor in the spread of infectious disease through human populations. In the presence of increasing infection risk, individuals typically engage in protective behaviors to avoid becoming ill. These preventative behavior changes may be imposed by a governing body (e.g., city-wide lockdowns or school closures), or may be the result of personal choices (e.g., social distancing or voluntary masking). Behavioral change can have a substantial impact on the epidemic trajectory by delaying the peak, reducing the total number of individuals that contract the disease, and/or resulting in multiple waves of transmission. Additionally, behavioral change is dynamic; higher disease prevalence tends to result in increased preventative measures, which are subsequently relaxed as prevalence decreases. Understanding these changes in population behavior in response to an epidemic is crucial for public health practitioners and policy makers attempting to stop or slow the spread of the pathogen and allocate valuable resources.

Statistical modeling of infectious disease transmission provides a quantitative approach to understanding disease dynamics. The conventional methodology is based on the compartmental SIR model [1], which segments the population into **S**usceptible, **I**nfectious, and **R**emoved compartments capturing the important disease states. The model is then parameterized in terms of the rates of flow between compartments. Compartmental models can be implemented deterministically using ordinary differential equations or stochastically, with statistical inference typically carried out

*Corresponding author: ward-c@umn.edu

using Bayesian methodology. However, the traditional SIR model does not naturally account for transmission dynamics changing in real time as the population reacts to the outbreak, limiting its applicability to real epidemic data.

Previous work incorporating behavioral change into the SIR model framework has been done in the deterministic setting, with models generally falling into one of three categories. One approach adds additional “adherence” or “awareness” compartments to capture reductions in susceptibility and transmissibility for individuals engaging in protective behaviors [2, 3, 4, 5]. In these models, the rate at which individuals transition into the “adherence” compartments depends on recent disease prevalence with individuals more likely to be adhering to preventative measures when prevalence is high. Another popular method uses a game-theoretic approach, supplementing the SIR model with a time-varying utility function [6, 7]. The utility function balances costs associated with prevention strategies (monetary, liberty, social) with the benefit of lowering infection risk in the population, with costs and benefits changing over time in relation to the current infection prevalence. The remaining approach allows the transmission rate in the SIR model to be dynamically modified as a function of the recent disease trajectory [8, 9, 10, 11, 12].

Despite this large body of literature on incorporating behavioral change in epidemic models, there are still several unanswered questions. First, can these deterministic approaches be translated to the stochastic Bayesian setting? The Bayesian paradigm offers the ability to impute partially observed epidemic data and incorporate prior knowledge about the disease process. However, many of the proposed models include highly detailed depictions of behavioral dynamics and stochastic Bayesian models often require simpler parameterizations than their deterministic counterparts to be computationally tractable [13]. It is likely challenging to implement the more complicated models in the Bayesian framework without detailed behavioral data. Second, can disease and behavioral change parameters be estimated from epidemic data? The aforementioned modeling efforts have focused almost entirely on model specification, with primary results coming from forward simulations using pre-specified parameter values. Notably absent in the literature is any assessment of the statistical properties of these models when fit to real data. Finally, what practical considerations arise when using these models to increase understanding of human behavior during an epidemic?

In this article, we advance the field of stochastic infectious disease modeling by answering these important questions. We accomplish this by proposing a novel Bayesian SIR model formulation which captures dynamic behavioral change during an epidemic. The proposed model specifies the transmission rate as a function of recent disease occurrence, and computation is performed via Markov Chain Monte Carlo (MCMC) methods. In our simulation study, we thoroughly investigate the statistical properties of our Bayesian model when fit to data. In particular, we show that behavioral change parameters can be accurately estimated and that posterior predictions from the proposed model can detect subsequent peaks in incidence. The model is then applied to COVID-19 data from New York City to assess behavioral change throughout the ongoing pandemic and illustrate important considerations when using the model in practice.

2 Methods

2.1 Traditional SIR Model

We model transmission using a discrete-time SIR model framework, where susceptible individuals can contract the infection from those who are infectious, and infectious individuals are removed when they no longer transmit the pathogen to others, due to death, isolation, or recovering with immunity. Let $t = 1, \dots, \tau$ indicate discrete calendar time and S_t , I_t , and R_t denote the number of individuals in the susceptible, infectious, and removed compartments in the continuous time interval $[t, t + 1)$, respectively. Furthermore, define the transition vectors I_t^* and R_t^* to represent the number of individuals entering the indicated compartment in this interval. Compartment membership is temporally described by the set of difference equations:

$$S_{t+1} = S_t - I_t^* \tag{1}$$

$$I_{t+1} = I_t + I_t^* - R_t^* \tag{2}$$

$$R_{t+1} = R_t + R_t^* \tag{3}$$

We assume a closed population, such that $S_t + I_t + R_t = N$ at all time points, where N denotes the total population size. Given the population size, a set of initial conditions, and the transition vectors, the compartment membership vectors can be fully determined using Equations 1 - 3.

In the Bayesian framework, we must establish the relationship between data and model parameters using probability distributions. We define the transitions between compartments to be binomially distributed [14, 15], such that $I_t^* \sim \text{Bin}(S_t, \pi_t^{(SI)})$ and $R_t^* \sim \text{Bin}(I_t, \pi_t^{(IR)})$. The transition probabilities $\pi_t^{(SI)}$ and $\pi_t^{(IR)}$ describe transmission of the pathogen and the duration of the infectious period, respectively. Assuming an independent Poisson contact process between individuals and constant probability of infection given a contact, the transmission probability, $\pi_t^{(SI)}$, takes the form

$$\pi_t^{(SI)} = 1 - \exp\left(-\beta \frac{I_t}{N}\right). \quad (4)$$

The parameter β is interpreted as the transmission rate, which captures both the contact rate and the infection probability, as these are not separately identifiable [16]. The removal probability, $\pi_t^{(IR)}$, is derived by assuming the length of time an individual is infectious is exponentially distributed with rate γ . In discrete time, $\pi_t^{(IR)}$ is the conditional probability of transitioning on day $s + 1$, given the individual has remained infectious through time s , resulting in $\pi_t^{(IR)} = 1 - \exp(-\gamma)$. The parameter γ is referred to as the removal rate, however, it is typically more interpretable to consider $1/\gamma$, the mean length of the infectious period.

The traditional SIR model assumes β is constant over time, however this is not realistic for most epidemics. More likely, transmission changes as the population responds to the outbreak. Seasonal factors may also contribute, such as the start of the school year or changes in weather. This can be incorporated by modifying the transmission probability from Equation 4 as

$$\pi_t^{(SI)} = 1 - \exp\left(-\beta_t \frac{I_t}{N}\right), \quad (5)$$

where β_t is the transmission rate at time t . Changes in transmission can be modeled directly through covariates, such as change points corresponding to the timing of government intervention(s) [15, 17] or measures of population mobility [18, 19], which allow inference to be made on the relationship between covariate(s) and transmission. Covariates might not capture all important changes in transmission, so more flexible approaches have been proposed, including basis splines [16, 20], Gaussian processes [21], or simple random walks [22]. All of these approaches are limited when forecasting, as it is difficult to predict when a government lockdown will be lifted, and restrictive assumptions must be made to allow any flexibly modeled trajectory of β_t to continue into the future. Thus, an alternate approach accounting for the mechanism of behavioral change is needed.

2.2 Behavioral Change (BC) Model

The proposed behavioral change (BC) model allows for time-varying transmission which captures behavioral change via a dynamically structured dependence on previously observed epidemic trajectory. This is accomplished by allowing a constant transmission rate, β , to be modified by a time-varying level of alarm in the population, denoted a_t , such that $\beta_t = \beta(1 - a_t)$. We consider $a_t \in [0, 1]$, such that a_t corresponds to the proportional reduction in transmission due to the alarm in the population. When $a_t = 0$, the population is in its natural ‘unalarmed’ state, and transmission is described only by β . When $a_t = 1$, the population is in its maximal alarmed state and transmission is reduced to zero. Plugging this in to Equation 5 yields

$$\pi_t^{(SI)} = 1 - \exp\left[-\beta(1 - a_t) \cdot \frac{I_t}{N}\right]. \quad (6)$$

The structural dependence in the alarm is captured by specifying a_t as a function of incidence smoothed over the past m days, such that $a_t = f\left(\frac{1}{m} \sum_{i=t-m-1}^{t-1} I_i^*\right)$ and the smoothing parameter $m \in \{1, 2, \dots, t-1\}$. For $t < m$, we use the moving average of the data up until time $t - 1$, e.g., at time $t = 3$ the alarm is based on the average of the incidence observed at times $t = 1$ and 2. At the start of an epidemic, it is assumed that the alarm is zero. While its possible for

the alarm function to depend on other reported metrics of epidemic severity, such as prevalence, hospitalizations, or test positivity rates, here we will focus on an incidence-based alarm. Incidence is advantageous for forecasting, as it is directly generated from the SIR model. Thus, incidence forecasts can be used directly to determine future alarm function values and generate further predictions.

Next, we must determine an appropriate functional form for the alarm function. As defined, the alarm must be between 0 and 1, and furthermore we would expect the alarm to be zero when there is no disease in the population, and to monotonically increase as the amount of disease in the population increases. There are many functions that satisfy these characteristics, and we investigate three possibilities of various complexity (Figure 1). The first function considered is a one-parameter function $f(x) = 1 - (1 - x/N)^{1/k}$ used in previous deterministic literature [10, 12], which we will call the “power” alarm. The parameter $k > 0$ describes the growth rate, with smaller values corresponding with a faster rise in alarm. The next function we consider is a two-parameter constant change point model, which we call the “threshold” alarm and specify as $f(x) = \delta \mathbb{1}(x > H)$. The threshold alarm is zero until the threshold, H , is surpassed, at which point it becomes δ . H can take on any value in the observed range of the data informing the alarm function and $\delta \in [0, 1]$. The final function analyzed is a modified Hill equation [23], $f(x) = \frac{\delta}{1 + (x_0/x)^\nu}$, which we refer to as the “Hill” alarm. With three parameters, the Hill alarm is the most complex of the three alarm functions considered; $\delta \in [0, 1]$ describes the asymptote, x_0 is the half occupation value, and $\nu > 0$ controls the growth rate. The Hill alarm can describe curves similar to the power alarm, as well as sigmoid-shaped curves that resemble a smoothed version of the threshold alarm.

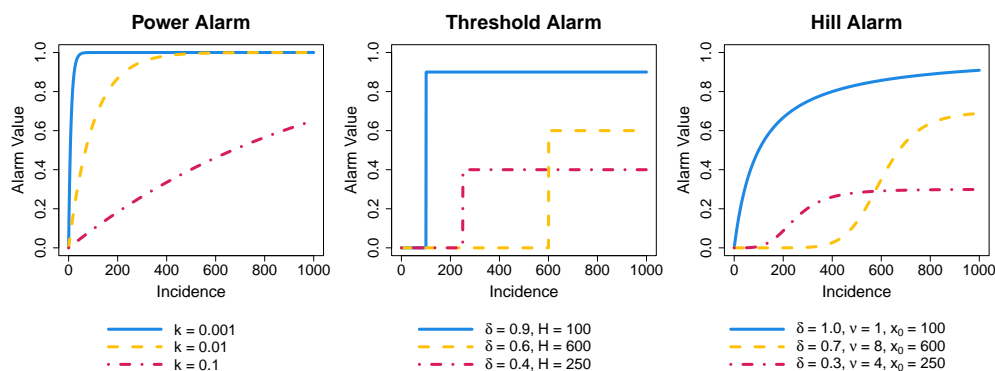


Figure 1: Example alarm functions for various parameter specifications.

These alarm functions can generate a multitude of epidemics. Figure 2a shows that higher levels of alarm reduce peak incidence. In addition, increasing the maximum alarm value in the threshold and Hill alarms delays the peak, while increasing the growth rate of the power alarm does not affect the timing of the initial peak. Figure 2b illustrates epidemics generated from alarms which reach high values at relatively low levels of incidence, as well as how epidemic trajectory is affected by the amount of data informing the alarm function. When the alarm is based solely on the previous day’s incidence, incidence becomes volatile and oscillates between levels producing high and low amounts of alarm. Peaks become more pronounced and spread out when the 14 or 30-day average incidence is used to inform the alarm. Finally, the threshold alarm, which reaches its maximum instantaneously, leads to epidemic curves with very sharp peaks. In contrast, the power and Hill alarm increase gradually, resulting in smoother peaks.

In practice, it may not be obvious which alarm function to use. For this reason, we also investigate the use of more flexible non-parametric approaches to estimating the alarm function using basis splines and Gaussian processes. The spline alarm is modeled using natural cubic splines with estimated knot locations and written as $f(x) = \mathbf{X}_B \mathbf{b}$. The basis matrix, \mathbf{X}_B , is constructed across the range of observed m -day average incidence and \mathbf{b} denotes the associated basis parameters. Constraints were used during estimation to ensure $f(x) \in [0, 1]$, but an appropriate link function (e.g., logit) could also be used. For the Gaussian process approach, we assume the logit of the alarm function is a realization from a multi-variate normal distribution which is fully specified by its mean $m(x)$ and covariance $k(x, x')$,

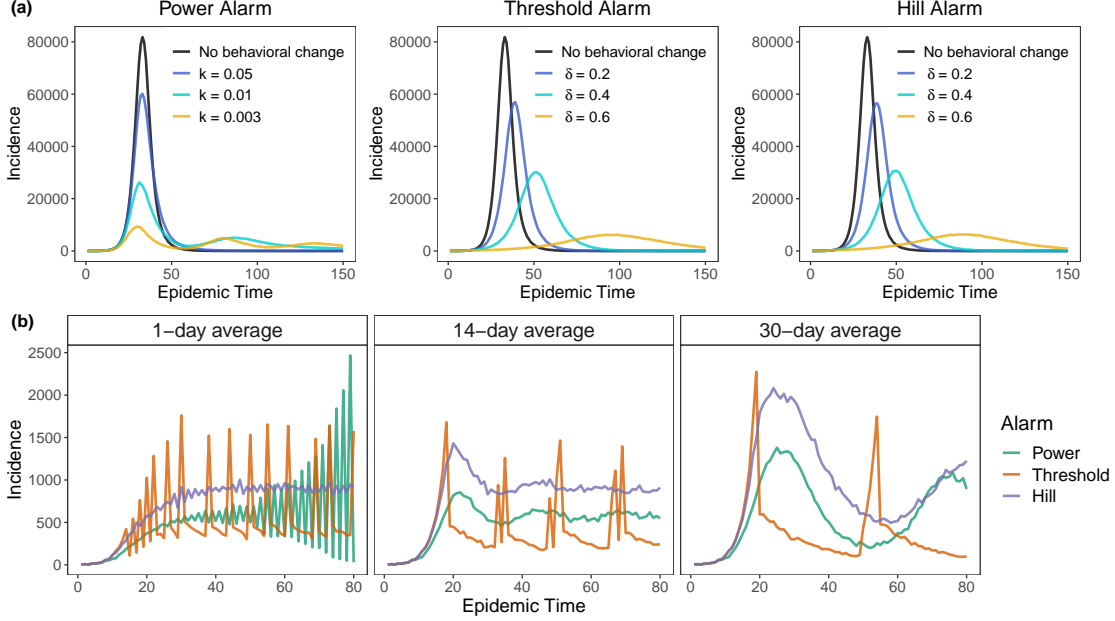


Figure 2: Example simulated epidemics for various alarm function specifications. (a) Compared to epidemics with no behavioral change, the power alarm with various k values, the threshold alarm with $H = 100$ and various δ values, and the Hill alarm with $\nu = 5$, $x_0 = 100$, and various δ values. Across all simulations, $\beta = 0.6$ and $\gamma = 0.2$. (b) Using 1-day, 14-day, and 30-day average incidence to inform the alarm function. Across the smoothing levels, the power alarm has $k = 0.0005$, the threshold alarm has $\delta = 0.8$ and $H = 350$, and the Hill alarm has $\delta = 0.85$, $\nu = 2$, and $x_0 = 450$. Across all simulations, $\beta = 0.6$ and $\gamma = 0.2$.

i.e., $\text{logit}[f(x)] \sim \text{MVN}[m(x), k(x, x')]$. We specify the mean function to start at $(0, 0)$ and end at $(\max(x), 1)$ on the logit scale, corresponding with the characteristics we expect of the alarm function. As we generally expect the alarm function to be smooth, we use the squared exponential covariance function $k(x, x') = \sigma^2 \exp[-(x - x')^2/2l^2]$, where $\sigma^2 > 0$ is the signal variance controls scaling and $l > 0$ is the length-scale parameter controlling smoothness. Both alarms are defined across the range of observed m -day average incidence, so linear interpolation was used to find the value of the alarm on each day.

One of the most important quantities estimated by epidemic models is the reproductive number, denoted \mathcal{R}_0 , which quantifies the spread of the pathogen in the population. Various methods of calculating \mathcal{R}_0 exist, and we use the approach of [24]. The effective reproductive number is calculated as $\mathcal{R}_0(t) = S_t \sum_{k=t}^{\infty} [1 - \exp(-\beta_k/N)] \exp(-\gamma)^{k-t}$ and provides the expected number of secondary infectious caused by a single individual that becomes infectious at time t (for the full derivation, see [24]). \mathcal{R}_0 can be interpreted in relation to the threshold of 1, as $\mathcal{R}_0 \geq 1$ means the epidemic will continue to propagate through the population and $\mathcal{R}_0 < 1$ indicates the epidemic will eventually die out.

2.3 Bayesian Estimation and Implementation

The complete log-likelihood for the chain binomial SIR model is

$$\begin{aligned} \ell(\mathbf{I}^*, \mathbf{R}^* | \Theta) = \sum_{t=0}^{\tau} \left[\log \binom{S_t}{I_t^*} + I_t^* \log \pi_t^{(SI)} + (S_t - I_t^*) \log \left(1 - \pi_t^{(SI)} \right) \right. \\ \left. + \log \binom{I_t}{R_t^*} + R_t^* \log \pi^{(IR)} + (I_t - R_t^*) \log \left(1 - \pi^{(IR)} \right) \right], \end{aligned} \quad (7)$$

where the parameter vector Θ contains β and γ for the traditional model, and includes additional parameters used to estimate β_t for the time-varying transmission models and the BC model. Complete data would provide the time

series over the course of the epidemic for the transition vectors \mathbf{I}^* and \mathbf{R}^* , the initial conditions S_0 and I_0 , and the population size N . Often, we do not observe complete information on infectious and removal times. Throughout this work, we assume that incidence (\mathbf{I}^*) is observed, and removals (\mathbf{R}^*) must be imputed, using data augmented MCMC methods [25, 15]. The R package `nimble` [26, 27] was used for computation, as it offers a mechanism for implementing user-defined data augmented MCMC algorithms.

In the Bayesian framework, the parameter vector must be assigned a prior, with the use and justification of informative priors for any parameters varying by disease application. Often, the gamma distribution is used to specify the prior for β and γ as both parameters must be positive. In the presence of knowledge about the duration of the infectious period, informative priors can be used for γ . Determining informative priors for the parameters of the alarm functions is challenging. We use a vague gamma prior for k in the power alarm and $\text{Uniform}(0, 1)$ priors for δ in the threshold and Hill alarms. For H and x_0 $\text{Uniform}(\min(x), \max(x))$ priors are used as we expect the change point or half occupation point to occur during the observed range of incidence. The spline coefficients \mathbf{b} are given vague $N(0, 100)$ priors and the knots are given $\text{Uniform}(\min(x), \max(x))$ priors. The parameters of the covariance in the Gaussian process model, σ and l are weakly identified [28], making the use of informative priors crucial. As the alarm function is estimated on the logit scale, the variability of the function is limited, so we use a $\text{gamma}(150, 50)$ prior for σ . The prior for the length-scale parameter was specified as inverse gamma with the shape and scale parameters determined using the practical range approach [29]. Using this approach, the mean of the prior for l is specified by finding the value such that the covariance function is 0.05 for two points that are separated by half the maximum distance observed in the data. The prior standard deviation was fixed at two, as that was found to produce reasonable estimation.

3 Simulation Study

3.1 Simulation set-up

The statistical properties of the BC model are assessed via simulation. The primary goal of the simulation study was determining whether the behavioral change mechanism could be recovered through estimation of the alarm function. The secondary objective was comparing the BC model to the traditional approach without behavioral change and a flexible time-varying transmission model, assessing posterior predictive forecasting and model fit. These aims were addressed by simulating epidemics with behavioral change under the three alarm functions described in Section 2.2. For each of the three data generation scenarios, 50 epidemics were simulated using the initial conditions $N = 1,000,000$, $S_0 = 999,995$, and $I_0 = 5$. Five models were fit to each simulated epidemic: a BC model using the true alarm function, BC models using the spline and Gaussian process alarms, the model with no behavioral change, and a time-varying transmission model with β_t estimated flexibly using natural cubic splines.

To evaluate posterior prediction, epidemics were simulated over 100 days, with the first 50 days used for model fitting and the subsequent 50 days used to evaluate forecasting accuracy. Simulation parameters were chosen to produce epidemics with a distinguished peak during the first 50 days of the epidemic and with additional peak(s) occurring in the subsequent 50 days. Complete specification of simulation parameters is provided in Supplementary Table 1. Epidemics were generated and BC models were fitted using both 14-day and 30-day average incidence to inform the alarm function. Similar conclusions were found in both settings, so we detail the 30-day average results here and provide the 14-day average results in the Supplementary Material.

Priors were specified as described in Section 2.3. For each model, three MCMC chains were run using various starting values of the parameters. The BC models and the flexible β_t model required more burn-in iterations due to their increased complexity. All models were run for 300,000 iterations post burn-in with samples drawn every 10th iteration. Full descriptions of priors used and MCMC specifications are provided in Supplementary Table 2. Convergence was established by a Gelman and Rubin diagnostic value below 1.1 [30]. A small number of models did not converge despite running for a large number of iterations and have been excluded from the results. More information on these models is provided in the Supplementary Material.

3.2 Simulation results

3.2.1 Alarm function estimation

To assess estimation of the alarm function in each data generating scenario, we compare posterior mean alarm function estimates to the true alarm functions (Figure 3). The alarm is shown as a function of the 30-day average incidence, ranging from zero to the maximum observed value during the epidemic, which varies between simulations. We find estimation of the alarm function to be excellent when the true functional form of the alarm was used in model fitting. More interestingly, we find the spline and Gaussian process approaches recover the alarm function reasonably well, particularly for the power and Hill alarms. The alarm function recovery is not as precise when the threshold alarm is the true function. However, this is expected as the piecewise constant form of this alarm is generally not well described by splines or Gaussian processes, which are inherently smooth. Despite this, both approaches are able to detect the alarm function rapidly increasing and leveling off quite impressively. These results indicate that when analyzing real data where the true alarm function is unknown, the spline and Gaussian process alarms offer robust and flexible possibilities.

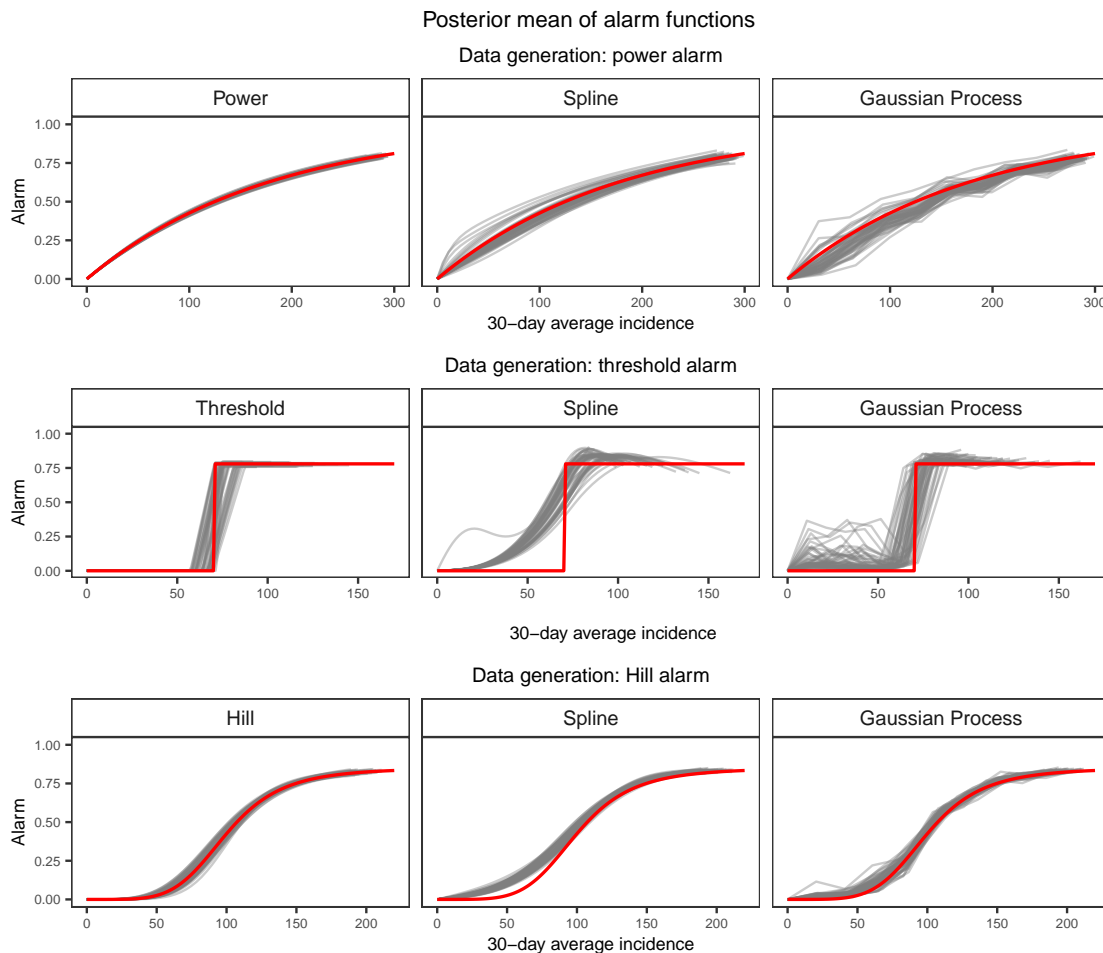


Figure 3: True and posterior mean estimates of alarm functions from 50 simulated epidemics using the correct parametric alarm function, and the spline and Gaussian process alarms for model fitting. True alarm functions shown in red.

3.2.2 Posterior prediction

The ability of the fitted BC models to predict the epidemic curve was carried out using the posterior distribution for model parameters derived using the first 50 days of the epidemic. For 10,000 posterior draws of the parameters, the future epidemic trajectory was simulated using the model state on day 50 to determine the initial values and proceeding with binomial draws from S_t and I_t for $t = 51, \dots, 100$. A drawback of the flexible β_t model is there is no obvious mechanism for forecasting, so we compare the model with no behavioral change to the three BC models (true, spline, and Gaussian process alarms). Consistent results were found across simulations. For brevity, the posterior predictive distribution is provided for a single, randomly selected, and typical simulation in Figure 4.

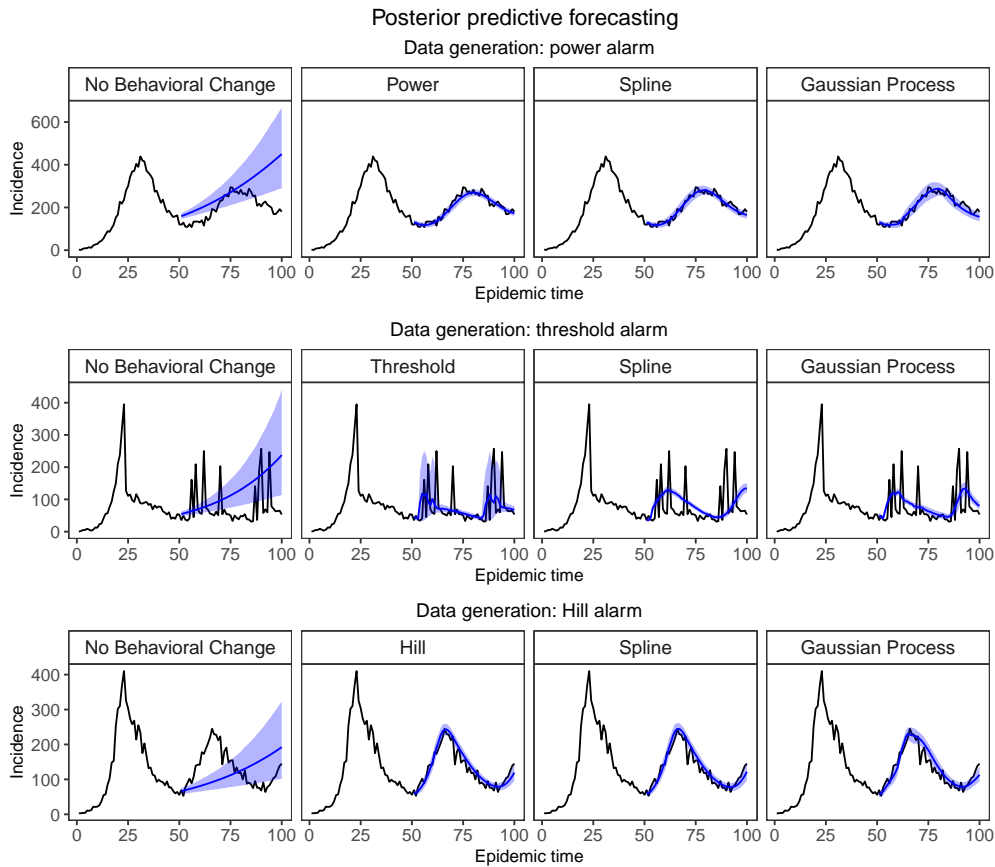


Figure 4: Mean and 95% credible intervals for posterior predictive forecasts of future incidence compared to the truth for a randomly selected simulation.

The model which does not incorporate behavioral change does a poor job of posterior prediction. Assuming constant transmission yields an estimated β which averages over what was observed during the first 50 days. Correspondingly, the posterior predictive trajectories are increasing, but at a slower rate than the growth observed at the start of the epidemic. In contrast, posterior predictions from the BC models are able to detect the intensity and timing of subsequent waves of transmission. Minimal differences were found between predictions from the parametric and non-parametric approaches for data generated with the power and Hill alarms. For epidemics simulated using the threshold alarm, the non-parametric approaches predict smoother subsequent peaks, due to their failure to capture the abruptness of the change point in the alarm. Finally, the 95% posterior credible intervals for the model with no behavioral change widen as predictions become further from the last observed time point. This is not seen for the BC models, as the structural dependency encoded by the alarm function restricts the shape of the epidemic curve.

3.2.3 Comparing model fit

Model fit was assessed with the Widely Applicable Information Criteria (WAIC) [31], for which lower values indicate superior model fit. The distribution of WAIC values and the proportion of epidemics where each model had the lowest WAIC are summarized in Table 1. The true alarm function was selected 82 - 96% of the time, indicating that WAIC is able to correctly identify the best model. The spline and Gaussian process BC models sometimes provided the best fit. This was less likely when the data was generated from the threshold alarm, where recovery of the alarm function by these methods was poorest. Notably, despite its flexibility, the time-varying β_t model was only selected once and generally had higher average WAIC than any of the BC models. The exception was for data generated from the power alarm, the most gradual alarm function. This indicates that the additional structure imposed by the BC models results in lower WAIC in the simulation setting where data was generated from a model with behavioral change present. The traditional model with no behavioral change performs poorly across all three data generation scenarios.

Table 1: Summaries of WAIC values across 50 simulated epidemics from three data generation scenarios. Models are ordered by mean WAIC.

Data generation	Model fitted	WAIC Mean (SD)	% selected
Power	Power	369.63 (12.80)	92%
	Spline	371.43 (12.73)	8%
	β_t	375.28 (13.19)	0%
	Gaussian process	381.44 (13.78)	0%
	No Behavioral Change	673.74 (16.25)	0%
Threshold	Threshold	333.19 (12.61)	96%
	Gaussian process	367.06 (48.96)	4%
	Spline	484.39 (65.67)	0%
	β_t	720.61 (59.87)	0%
	No Behavioral Change	1058.45 (120.73)	0%
Hill	Hill	358.55 (13.61)	82%
	Spline	360.28 (13.33)	10%
	Gaussian process	364.06 (13.95)	6%
	β_t	375.39 (19.04)	2%
	No Behavioral Change	793.40 (34.11)	0%

4 Data Application - COVID-19

4.1 Background

After the first cases of COVID-19 were identified in China in December 2019, the SARS-CoV-2 virus spread rapidly across the globe, being declared a pandemic by the World Health Organization in March 2020 [32]. Although many cases of COVID-19 have mild to moderate respiratory symptoms, severe symptoms can lead to death, with over 6.5 million deaths from COVID-19 having been reported at the time of writing [33]. Throughout the pandemic, the importance of incorporating behavioral change in epidemic models has been accentuated as governments impose/relax various restrictions over time leading to multiple waves of incidence. New SARS-CoV-2 variants have emerged, changing important characteristics of the virus such as its transmissibility, vaccine efficacy, and disease severity [34]. We illustrate the use of the BC model to capture these features using COVID-19 data from New York City (NYC) from March 2020 - November 2021. The data used for this study are publicly available as part of the NYC Department of Health and Mental Hygiene Github repository [35]. Based on the observed case counts, we define three waves of COVID-19 in NYC to be analyzed (Figure 5). For the purposes of our analysis, we exclude the incidence occurring after the highly contagious Omicron variant became dominant in NYC, as the epidemic dynamics changed drastically at this time, including increased use of at-home rapid tests not reported in official data, higher vaccine resistance of the variant, and higher likelihood of reinfection.

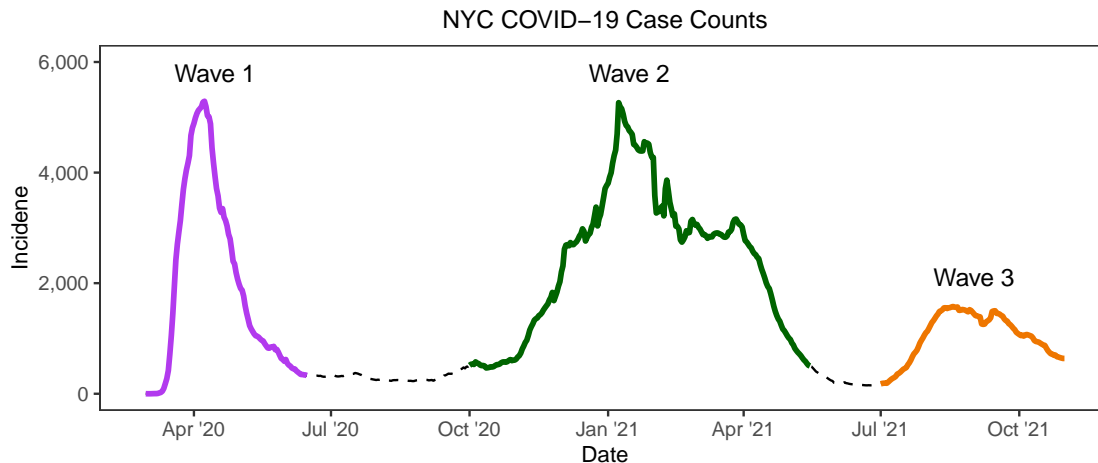


Figure 5: New York City COVID-19 data and waves defined for the analysis. Wave 1 occurs between Mar 1 and Jun 15 2020, Wave 2 between Oct 1, 2020 and May 15, 2021, and Wave 3 between July 1 and Oct 31, 2021.

4.2 Analysis

To evaluate the various BC model specifications, the power, threshold, Hill, spline, and Gaussian process alarms were all used to model the three COVID-19 waves. As in the simulation study, the model with no behavioral change and the flexible β_t model were also fitted for comparison purposes. Prior to model fitting, the reported counts of new cases over time were smoothed to the 7-day average to account for weekly fluctuations in reporting. We assume the smoothed incidence provides the time-series I^* , and use data augmented MCMC to estimate R^* . While we know this is not true because of under-reporting, this assumption allows the models to be computationally feasible and we argue the models are still useful for understanding behavioral change.

The population size was set as $N = 8,804,190$, the recorded population from the 2020 census. For each wave, we allow the initial conditions S_0 and I_0 to be estimated, using strong priors based on the past epidemic trajectory. Vague priors for β and the parameters of the alarm function and flexible spline model were specified as in Section 2.3. The prior for γ was specified to correspond with a mean infectious period of three days and 80% prior probability of the mean between 2 and 4 days. This corresponds with the typical length of time between an individual becoming contagious and testing positive and subsequently isolating. Results of a sensitivity analysis on this prior indicated little impact to the main conclusions across various priors and are provided in the Supplementary Material. Full specification of all priors for model parameters are detailed in Supplementary Table 9. The BC models were fit using both 30-day and 60-day average incidence to inform the alarm functions. Convergence was established by a Gelman and Rubin diagnostic value below 1.1 [30].

4.3 Results

To determine the best fitting models for each wave of the pandemic, WAIC values were compared (Table 2). Modeling β_t flexibly with splines provided the best fit to all three waves, which is not unexpected as the BC model is less flexible due to the alarm function specification. The Gaussian process, spline, and Hill alarms were among the BC models with the lowest WAIC across all three waves. For the first and third waves, using 60-day average incidence to inform the alarm function offered better model fit, while the 30-day average performed better for the second wave. This is likely due to the different shape of the epidemic curve during Wave 2, which peaked in the beginning of January 2021, but leveled off between March - April 2021 before incidence was truly driven down. In contrast, Waves 1 and 3 showed relatively steady declines in incidence post-peak, indicating the behavioral change in the population continued until the wave died out. The model with no behavioral change had the highest WAIC for Waves 1 and 3 and for Wave 2 had the second highest WAIC, indicating the importance of incorporating of behavioral change.

Table 2: WAIC values for all converged models used in the New York City COVID-19 analysis. Within each wave, models are ordered by WAIC. The BC models chosen for the final results are indicated in italics. The power alarm model did not converge for Wave 2 and is therefore excluded from these results.

Wave	Model fitted	Smoothing	WAIC
Wave 1	β_t	None	1089.83
	<i>Gaussian process</i>	<i>60-day</i>	1092.92
	Spline	60-day	1099.02
	Hill	60-day	1125.36
	Spline	30-day	1157.33
	Gaussian process	30-day	1157.89
	Hill	30-day	1190.37
	Threshold	30-day	1466.06
	Threshold	60-day	1466.34
	Power	60-day	1540.83
	Power	30-day	1753.43
No Behavior Change	None	2263.96	
Wave 2	β_t	None	2865.70
	<i>Gaussian process</i>	<i>30-day</i>	3025.92
	Threshold	30-day	3041.86
	Hill	30-day	3045.90
	Spline	30-day	3051.68
	Threshold	60-day	3078.72
	Hill	60-day	3080.96
	Gaussian process	60-day	3091.50
	No Behavior Change	None	3102.84
	Spline	60-day	3105.28
Wave 3	β_t	None	1155.36
	Spline	60-day	1170.35
	<i>Gaussian process</i>	<i>60-day</i>	1170.91
	Hill	60-day	1171.02
	Spline	30-day	1187.00
	Hill	30-day	1188.60
	Gaussian process	30-day	1195.00
	Threshold	30-day	1199.95
	Threshold	60-day	1200.35
	Power	60-day	1201.31
	Power	30-day	1208.86
No Behavior Change	None	1291.58	

Based on the WAIC results, we present the estimated alarm functions for each BC model based on 60-day average incidence for Waves 1 and 3, and 30-day average incidence for Wave 2 (Figure 6). Despite the restricted shapes of the parametric functions, the estimated alarm functions were generally similar. The spline and Gaussian process alarms were very alike, which is not surprising due to the relationship between Gaussian processes and splines [36]. The estimated alarm functions can be used to evaluate changes in pandemic response over time. During the first wave, the alarm reached very high levels at relatively low observed incidence. The second wave started while many restrictions from the first wave were still in place, and correspondingly the BC models estimate very slight increases in alarm at higher levels of observed incidence. The third wave occurred after New York state lifted many restrictions in June 2020 and the more transmissible delta variant emerged. Correspondingly, the estimated alarm functions reach higher levels than during the second wave, and do so at lower levels of observed incidence.

Finally, we compare estimated reproductive numbers and posterior predictive distributions between the BC model using the Gaussian process alarm, the flexible β_t model, and the model with no behavioral change (Figure 7). The Gaussian process alarm was chosen as it had the lowest WAIC of the BC models for Waves 1 and 2, and in Wave 3 had nearly identical WAIC to the best BC model. The posterior predictive distribution was computed using 10,000 posterior

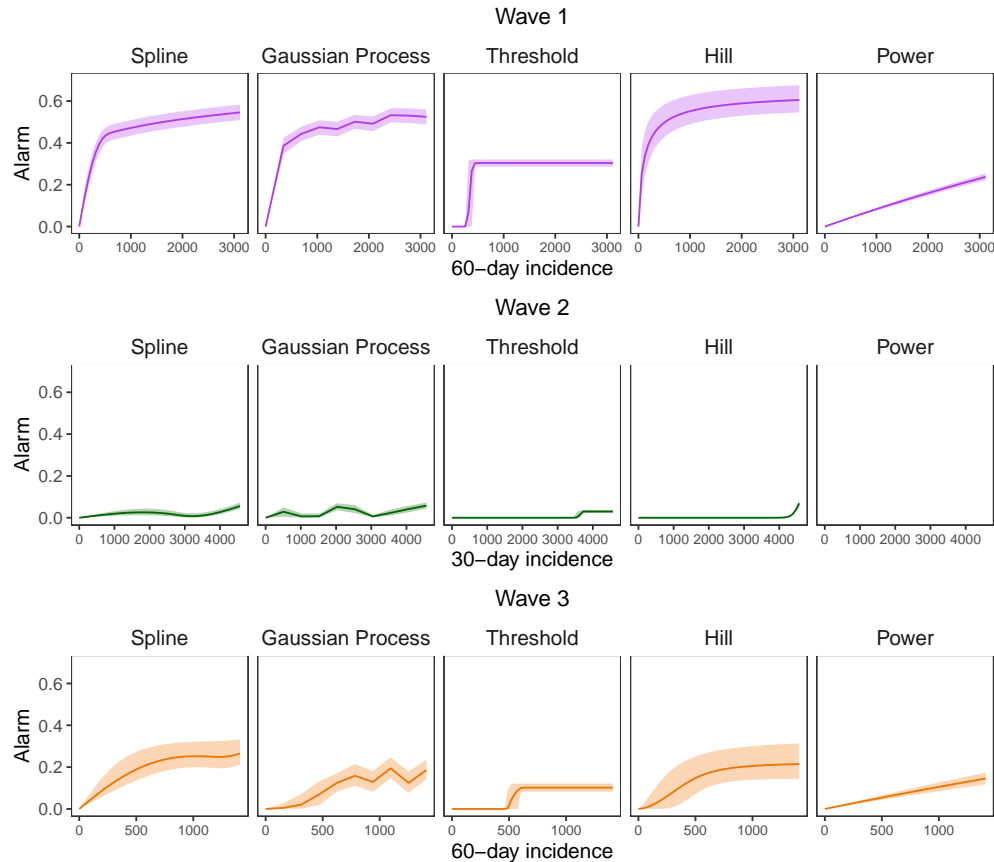


Figure 6: Posterior means and 95% credible intervals for all estimated alarm functions from each wave of the NYC COVID-19 epidemic. The power alarm model did not converge for Wave 2 and is therefore excluded from these results.

draws of the model parameters, which includes S_0 and I_0 . For each draw, the epidemic trajectory is simulated from the chain binomial model and is compared to the true observed epidemic curve.

For the first COVID-19 wave, the trajectory of $\mathcal{R}_0(t)$ is quite different between the three models, particularly between March and April 2020. The BC model estimates $\mathcal{R}_0(t)$ starting around 2, while the flexible β_t model estimates a higher value around 3, and the model with no behavioral change estimating $\mathcal{R}_0(t) \approx 1$ over the entire wave. This leads to vastly different posterior predictive distributions, due to the high variability in stochastic epidemic models at the start of an epidemic. Interestingly, the flexible β_t model has poor posterior predictive fit, despite having the lowest WAIC. This is likely because WAIC weights each time point equally in calculating the log predictive density, whereas the posterior predictive epidemic trajectory is highly influenced by the estimated $\mathcal{R}_0(t)$ at time one. In Wave 2, the estimated $\mathcal{R}_0(t)$ for the BC model and the no behavioral change model is just above 1 until mid-January 2021. The flexible β_t model follows a similar trajectory, except $\mathcal{R}_0(t)$ is below 1 for the first two days, which allows it to better capture the slow growth of the epidemic at the beginning of October 2020 in the posterior predictive trajectory. The BC model struggles with the shape of the epidemic curve in Wave 2, as incidence stops declining between March and April 2021. However, the posterior predictive distribution appears slightly better than that of the model with no behavioral change. In Wave 3, the BC and flexible β_t models estimate $\mathcal{R}_0(t)$ peaking just under 1.2 at the start of the wave and crossing below 1 in mid-August 2021. Both models have similar posterior predictive distributions which cover the true epidemic curve well. The model with no behavioral change again estimates $\mathcal{R}_0(t) \approx 1$ over the entire wave, and has very poor posterior predictive fit.

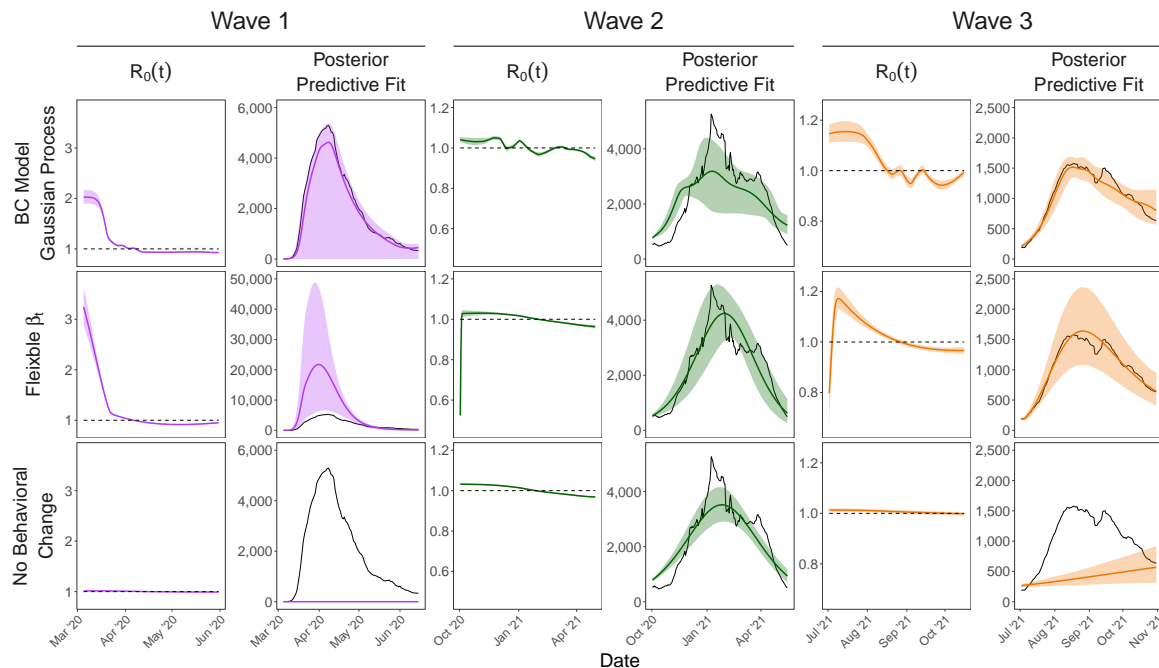


Figure 7: Posterior means and 95% credible intervals for the effective reproductive number of time and the posterior predictive distribution from each wave of the NYC COVID-19 epidemic. Results are presented for the BC model using the Gaussian process alarm, the flexible β_t model and the model with no behavioral change.

5 Discussion

There is a critical need to understand the dynamics of population behavior changing in response to an infectious disease outbreak. Guided by the previous deterministic literature, we developed a novel Bayesian behavioral change epidemic model framework which characterizes behavioral change dynamics at the population level while remaining simple enough to be computationally feasible. We showed that the proposed BC model can accurately estimate the mechanism of behavioral change across a wide range of scenarios, even when flexible non-parametric methods are used. The practical implications and usefulness of the proposed approach were illustrated with a highly relevant case study using COVID-19 data from New York City, although the model could be applied to any communicable disease. This work goes beyond previous behavioral change literature focused on model specification and simulation by using Bayesian inferential methods to estimate behavioral change and other model parameters exclusively from observed data.

Our simulation study conducted a thorough investigation of the BC model and made several notable findings. First, when behavioral change impacts epidemic trajectory, the BC model is able to accurately estimate the mechanism of behavioral change. We considered three different alarm functions to describe behavioral change, and although the functions impact the epidemic trajectory differently, we were able to reasonably capture all three functions using non-parametric splines and Gaussian processes. This is hugely beneficial, as it may be difficult to choose an appropriate functional form of the alarm when analyzing real epidemic data. We also showed that posterior predictive forecasts from the BC model can accurately detect a second peak, something that is not feasible with the traditional SIR model. Finally, WAIC provided an accurate metric for selecting the best fit model and we found the additional structure in the BC models generally lead to lower WAIC values than the more flexible approach of estimating β_t directly, even though both approaches are able to capture changes in transmission over time.

Our analysis of the COVID-19 epidemic in New York City offers numerous insights into behavioral change during the pandemic, but is subject to some limitations due to challenges arising from the nature of the available data and computational feasibility. The SIR model is a simplistic representation of highly complex dynamics, and does not

account directly for factors such as vaccination, waning immunity, under-reporting, or imperfect testing. Our primary analysis goal is illustrating the usefulness of the BC model and not creating the most realistic COVID-19 model possible. Even so, we argue that the simple model is still a useful tool for understanding behavioral change. In addition, the alarm function specification of the BC model could be incorporated into models with more complex structures when needed to achieve the analysis goals.

In this work we considered a population-average model which assumes homogeneous mixing and equal susceptibility for all members of the population. These assumptions may not be realistic, as factors like age are known to impact contact rates and susceptibility. Many extensions to the Bayesian SIR model have been introduced to relax these assumptions, including the use of a stratified population structure [37, 16], the addition of spatial random effects in the transmission rate [38, 39], or allowing the transmission rate to be impacted by individual-level covariates [40]. Establishing the BC model in the population-averaged framework is important as data are often limited, but ongoing work seeks to incorporate behavioral change into models with individual covariates and spatial structure. In a more precise model where susceptibility and contact patterns are estimated separately, the alarm function could modify either factor. The alarm function itself may also be modeled as a function of individual-level covariates. Additionally, one may consider both the transmission rate and the alarm function to vary spatially, and models incorporating spatial structure in the alarm function could estimate region-specific alarms.

The proposed framework models behavioral change implicitly by allowing transmission to depend only on the perceived amount of disease in the population. However, time-varying measures of population behavior (e.g., Google mobility reports) exist and could be used to incorporate behavioral change directly in the specification of the transmission rate [41, 42]. One disadvantage of this approach is it requires simulation of the behavioral change metric, which may be challenging. In contrast, transmission in the BC model is based on previous incidence, which is generated directly from the SIR model. Despite this issue, comparing an approach using mobility metrics to the BC model is a promising avenue for future work. Developments including *both* measures of mobility and an alarm function based on epidemic trajectory in the transmission rate would be particularly interesting. In this setting, one could examine whether the alarm function is able to detect “finer grain” behavioral change which may not be captured by mobility data, e.g., voluntary masking.

Acknowledgments

Funding for the project was provided by the Canadian Statistical Sciences Institute (CANSSI) Distinguished Postdoctoral Fellowship. This research was enabled in part by computational resources provided by the University of Calgary.

Software

Software in the form of R code, together with data used and complete documentation is available at <https://github.com/ceward18/epidemicBCM>.

References

- [1] William Ogilvy Kermack and Anderson G McKendrick. A contribution to the mathematical theory of epidemics. *Proceedings of the Royal Society of London. Series A, Containing papers of a mathematical and physical character*, 115(772):700–721, 1927.
- [2] Sara Del Valle, Herbert Hethcote, James M Hyman, and Carlos Castillo-Chavez. Effects of behavioral changes in a smallpox attack model. *Mathematical Biosciences*, 195(2):228–251, 2005.
- [3] Nicola Perra, Duygu Balcan, Bruno Gonçalves, and Alessandro Vespignani. Towards a characterization of behavior-disease models. *PloS one*, 6(8):e23084, 2011.
- [4] G. O. Agaba, Y. N. Kyrychko, and K.B. Blyuss. Mathematical model for the impact of awareness on the dynamics of infectious diseases. *Mathematical Biosciences*, 286:22–30, 2017.

- [5] Manuel Adrian Acuña-Zegarra, Mario Santana-Cibrian, and Jorge X Velasco-Hernandez. Modeling behavioral change and COVID-19 containment in Mexico: A trade-off between lockdown and compliance. *Mathematical Biosciences*, 325:108370, 2020.
- [6] Timothy C Reluga. Game theory of social distancing in response to an epidemic. *PLoS Computational Biology*, 6(5):e1000793, 2010.
- [7] Eli P Fenichel, Carlos Castillo-Chavez, M Graziano Ceddia, Gerardo Chowell, Paula A Gonzalez Parra, Graham J Hickling, Garth Holloway, Richard Horan, Benjamin Morin, Charles Perrings, et al. Adaptive human behavior in epidemiological models. *Proceedings of the National Academy of Sciences*, 108(15):6306–6311, 2011.
- [8] Vincenzo Capasso and Gabriella Serio. A generalization of the kermack-mckendrick deterministic epidemic model. *Mathematical Biosciences*, 42(1-2):43–61, 1978.
- [9] David Greenhalgh, Sourav Rana, Sudip Samanta, Tridip Sardar, Sabyasachi Bhattacharya, and Joydev Chattopadhyay. Awareness programs control infectious disease—multiple delay induced mathematical model. *Applied Mathematics and Computation*, 251:539–563, 2015.
- [10] Ceyhun Eksin, Keith Paarporn, and Joshua S Weitz. Systematic biases in disease forecasting—the role of behavior change. *Epidemics*, 27:96–105, 2019.
- [11] Joshua S Weitz, Sang Woo Park, Ceyhun Eksin, and Jonathan Dushoff. Awareness-driven behavior changes can shift the shape of epidemics away from peaks and toward plateaus, shoulders, and oscillations. *Proceedings of the National Academy of Sciences*, 117(51):32764–32771, 2020.
- [12] Elisa Franco. A feedback SIR (fSIR) model highlights advantages and limitations of infection-based social distancing. *arXiv preprint arXiv:2004.13216*, 28, 2020.
- [13] Hakan Andersson and Tom Britton. *Stochastic Epidemic Models and their Statistical Analysis*, volume 151. Springer Science & Business Media, 2012.
- [14] Edwin B Wilson and Mary H Burke. The epidemic curve. *Proceedings of the National Academy of Sciences of the United States of America*, 28(9):361, 1942.
- [15] Pheny E Lekone and Bärbel F Finkenstädt. Statistical inference in a stochastic epidemic SEIR model with control intervention: Ebola as a case study. *Biometrics*, 62(4):1170–1177, 2006.
- [16] Grant D Brown, Jacob J Oleson, and Aaron T Porter. An empirically adjusted approach to reproductive number estimation for stochastic compartmental models: A case study of two Ebola outbreaks. *Biometrics*, 72(2):335–343, 2016.
- [17] Caitlin Ward, Grant D Brown, and Jacob J Oleson. An individual level infectious disease model in the presence of uncertainty from multiple, imperfect diagnostic tests. *Biometrics*, 2021.
- [18] Luyang Liu, Sharad Vikram, Junpeng Lao, Xue Ben, Alexander D’Amour, Shawn O’Banion, Mark Sandler, Rif A Saurous, and Matthew D Hoffman. Estimating the changing infection rate of COVID-19 using Bayesian models of mobility. *medRxiv*, 2020.
- [19] B Sartorius, AB Lawson, and RL Pullan. Modelling and predicting the spatio-temporal spread of COVID-19, associated deaths and impact of key risk factors in England. *Scientific Reports*, 11(1):1–11, 2021.
- [20] Hyokyung G Hong and Yi Li. Estimation of time-varying reproduction numbers underlying epidemiological processes: A new statistical tool for the COVID-19 pandemic. *PloS one*, 15(7):e0236464, 2020.
- [21] Xiaoguang Xu, Theodore Kypraios, and Philip D O’Neill. Bayesian non-parametric inference for stochastic epidemic models using Gaussian processes. *Biostatistics*, 17(4):619–633, 2016.
- [22] Nicholas J Irons and Adrian E Raftery. Estimating sars-cov-2 infections from deaths, confirmed cases, tests, and random surveys. *Proceedings of the National Academy of Sciences*, 118(31), 2021.
- [23] Rudolf Gesztelyi, Judit Zsuga, Adam Kemeny-Beke, Balazs Varga, Bela Juhasz, and Arpad Tosaki. The hill equation and the origin of quantitative pharmacology. *Archive for History of Exact Sciences*, 66(4):427–438, 2012.

- [24] Caitlin Ward, Grant D Brown, and Jacob J Oleson. Incorporating infectious duration-dependent transmission into bayesian epidemic models. *Biometrical Journal*, 2022.
- [25] Philip D O’Neill and Gareth O Roberts. Bayesian inference for partially observed stochastic epidemics. *Journal of the Royal Statistical Society: Series A (Statistics in Society)*, 162(1):121–129, 1999.
- [26] P. de Valpine, D. Turek, C.J. Paciorek, C. Anderson-Bergman, D. Temple Lang, and R. Bodik. Programming with models: writing statistical algorithms for general model structures with NIMBLE. *Journal of Computational and Graphical Statistics*, 26:403–417, 2017.
- [27] P. de Valpine, C. Paciorek, D. Turek, N. Michaud, C. Anderson-Bergman, F. Obermeyer, C. Wehrhahn Cortes, A. Rodríguez, D. Temple Lang, S. Paganin, and J. Hug. NIMBLE: MCMC, particle filtering, and programmable hierarchical modeling, 2021.
- [28] Hao Zhang. Inconsistent estimation and asymptotically equal interpolations in model-based geostatistics. *Journal of the American Statistical Association*, 99(465):250–261, 2004.
- [29] Alan E Gelfand, Athanasios Kottas, and Steven N MacEachern. Bayesian nonparametric spatial modeling with dirichlet process mixing. *Journal of the American Statistical Association*, 100(471):1021–1035, 2005.
- [30] Andrew Gelman, Donald B Rubin, et al. Inference from iterative simulation using multiple sequences. *Statistical Science*, 7(4):457–472, 1992.
- [31] Sumio Watanabe and Manfred Opper. Asymptotic equivalence of bayes cross validation and widely applicable information criterion in singular learning theory. *Journal of Machine Learning Research*, 11(12), 2010.
- [32] WHO. WHO Director-General’s opening remarks at the media briefing on COVID-19 - 11 March 2020, 2020.
- [33] WHO. WHO Coronavirus (COVID-19) Dashboard, 2022.
- [34] WHO. Tracking SARS-CoV-2 variants, 2022.
- [35] NYC Health. Nyc coronavirus disease 2019 (covid-19) data. <https://github.com/nychealth/coronavirus-data>, 2022.
- [36] Grace Wahba. Improper priors, spline smoothing and the problem of guarding against model errors in regression. *Journal of the Royal Statistical Society: Series B (Methodological)*, 40(3):364–372, 1978.
- [37] Aaron T Porter and Jacob J Oleson. A spatial epidemic model for disease spread over a heterogeneous spatial support. *Statistics in medicine*, 35(5):721–733, 2016.
- [38] Andrew B Lawson and Joanne Kim. Space-time COVID-19 Bayesian SIR modeling in South Carolina. *PLoS One*, 16(3):e0242777, 2021.
- [39] MD Mahsin, Rob Deardon, and Patrick Brown. Geographically dependent individual-level models for infectious diseases transmission. *Biostatistics*, 23(1):1–17, 2022.
- [40] R. Deardon, S. P. Brooks, B. T. Grenfell, M. J. Keeling, M. J. Tildesley, N. J. Savill, D. J. Shaw, and M. E. Woolhouse. Inference for individual level models of infectious diseases in large populations. *Stat Sin*, 20(1):239–261, Jan 2010.
- [41] Fabio Vanni, David Lambert, Luigi Palatella, and Paolo Grigolini. On the use of aggregated human mobility data to estimate the reproduction number. *Scientific reports*, 11(1):1–10, 2021.
- [42] Tao Hu, Siqin Wang, Bing She, Mengxi Zhang, Xiao Huang, Yunhe Cui, Jacob Khuri, Yaxin Hu, Xiaokang Fu, Xiaoyue Wang, et al. Human mobility data in the covid-19 pandemic: characteristics, applications, and challenges. *International Journal of Digital Earth*, 14(9):1126–1147, 2021.